Contamination-Free Transmission Electron Microscopy for High-Resolution Carbon Elemental Mapping of Polymers

Shin Horiuchi,[†,*] Takeshi Hanada,[‡] Masaharu Ebisawa,[‡] Yasuhiro Matsuda,[§] Motoyasu Kobayashi,[§] and Atsushi Takahara[§]

[†]Nanotechnology Research Institute, National Institute of Advanced Industrial Science and Technology (AIST), 1-1-1, Higashi, Tsukuba, Ibaraki 305-8565, Japan, [‡]Consulting Zero Loss Imaging, Inc., 1-33-31, Shinkoji, Machida, Tokyo 195-0057, Japan, and [§]Institute for Materials Chemistry and Engineering, Kyushu University, 744 Motooka Nishi-ku, Fukuoka 819-0395, Japan

ABSTRACT Specimen contamination induced by electron beam irradiation has long been a serious problem for high-resolution imaging and analysis by a transmission electron microscope (TEM). It creates a deposition of carbonaceous compounds on a region under study, causing the loss of resolution. We developed a method to reduce the beam-induced specimen contamination by cleaning a TEM with activated oxygen radicals. The hydrocarbon contaminants accumulated inside the microscope's chamber can be etched away by gentle chemical oxidation without causing any damage to the microscope. The "contamination-free TEM" can effectively suppress the deposition of carbon-rich products on a specimen and therefore enables us to perform high-resolution carbon elemental mapping by energy-filtering transmission electron microscopy (EFTEM). In this study, we investigated the structure of polymer brushes immobilized on a silica nanoparticle (SiNP), of which molecular weight, length, and density of the brushes had been characterized in detail. The isolated particle showed the stretched formations of the polymer chains growing from the surface, while the densely distributed particles showed the connection of the polymer chains between neighboring particles. Moreover, the polymer brush layer and the surface initiator could be differentiated from each other by the component-specific contrast achieved by electron spectroscopic imaging (ESI). The contamination-free TEM can allow us to perform high-resolution carbon mapping and is expected to provide deep insights of soft materials' nanostructures.

KEYWORDS: transmission electron microscopy · polymer brush · elemental mapping · contamination · EFTEM

Transmission electron microscopy (TEM) has been an important tool for the characterization of nanoscale objects, which enables us to perform high-resolution imaging and also chemical composition and bonding studies. The developments in TEM imaging and analysis have contributed to the research and development of material science and engineering. Subangstrom imaging and analysis have become possible by the recent improvements of electron microscopes.[1,2] However, the spatial resolution associated with the imaging of soft materials, such as synthetic polymers, has its limitations mainly due to the radiation damage which causes the chemical and structural changes of a specimen. In contrast to the TEM studies of inorganic materials, where the spatial resolution is limited principally by the electron optics, the resolution limit of soft-materials imaging is governed by the total electron dose to which they can be exposed before undergoing structural changes.[3] Therefore, low-dose performances for the characterization of radiation-sensitive materials have been addressed and associated with parallel-beam nanodiffraction[4] and electron spectroscopic imaging using the low-loss portion of inelastically scattered electrons.[5−7]

The nanostructure characterizations of polymers have been employed by EFTEM due to its high detection sensitivity of light elements, which allows us to perform elemental mapping and electron energy loss spectroscopy (EELS).[8−11] Carbon is a predominant element in organic compounds, and thus the carbon analysis by EELS is expected to provide higher data collection efficiency than the other light elements. However, carbon analysis in polymers by EFTEM cannot successfully provide useful information on the polymer nanostructures. In addition to the radiation damage of a specimen, the contamination of the specimen induced by electron beam causes the uncertainty in the carbon analysis. It has been recognized that, in high-resolution imaging, contamination of a specimen causes loss of resolution.[3,12] The contamination is a carbonaceous layer deposited on the specimen surface as a result of electron bombardment. This beam-induced specimen contamination is caused by the hydrocarbons that are present in the chamber of a TEM. The electron beam reacts with stray hydrocarbons in the beam's path to create hydrocarbon ions which then condense

*Address correspondence to s.horiuchi@aist.go.jp.

Received for review February 17, 2009 and accepted April 21, 2009.

Published online April 29, 2009.
10.1021/nn9001598 CCC: $40.75

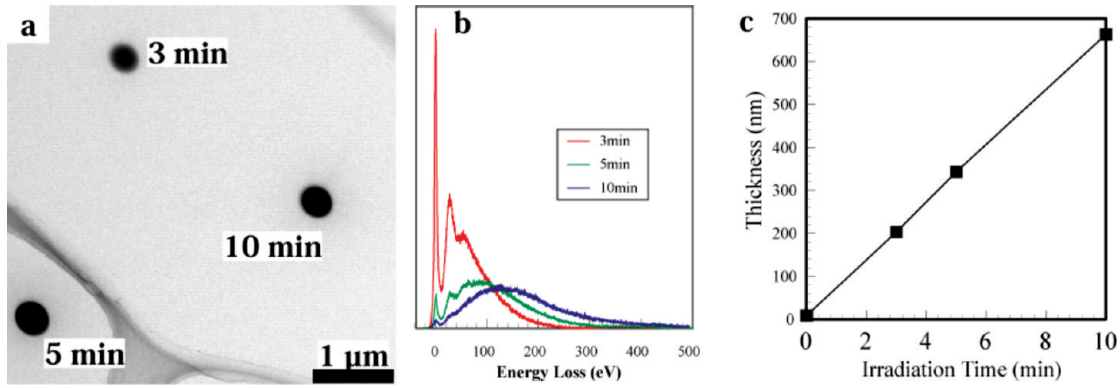

Figure 1. Beam-induced specimen contamination produced on a carbon thin foil by electron beam irradiation with an intensity of 5.6 × 10^4 el/nm · s. (a) TEM micrograph showing the contamination marks (dark spots) created by irradiation for 3, 5, and 10 min. (b) EELS spectra acquired from the contamination marks. (c) Thickness of the contamination marks estimated from the EELS spectra as a function of irradiation time.

and form carbon-rich polymerized film on the area being irradiated. The film may reach a level where it can be easily observed and eventually it can obscure the structural details of the specimen under study. The specimen contamination creates carbon-rich deposits on regions of interest in a specimen and disrupts the specimen-oriented carbon analysis and imaging. However, the influence of the specimen contamination on soft-materials imaging has not been discussed so much and has not yet been fully understood.

In this study, we attempted to remove hydrocarbon sources remaining in a TEM by gentle chemical etching with activated oxygen radicals produced in a plasma generator. Effective reduction of the specimen contamination with carbonaceous compounds will lead to the improvement of the quality and reliability of carbon elemental mapping and analysis. We investigated in this work the possibility of high-resolution carbon mapping of polymer brushes immobilized on a silica surface. The immobilization of polymers on a surface is a promising way of modifying the solid surface and providing various applications such as adhesion,[13] friction,[14] and photonic[15,16] and stimuli-responsive materials.[17] However, it has been difficult to observe the structures of polymer brushes in real space, which motivated us to observe the polymer brushes by EFTEM.

Electron-Beam-Induced Specimen Contamination. Figure 1a shows the contamination spots created on a 10 nm thick carbon thin foil by illuminating a beam with a diameter of about 200 nm and an intensity of 5.6 × 10^4 el/nm · s at an accelerating voltage of 200 kV for various periods. The thickness of contamination marks that are left by the electron beam can be estimated by EELS as shown in Figure 1b. The EELS spectra obtained from the contamination marks represent the significant increase in their thickness with increasing irradiation periods. With increase in the irradiation period, the intensity of the zero-loss peak decreases but the overall intensities in the energy-loss region of the spectra increase. The thickness (D) can be estimated using the equation, $D = \Lambda \cdot \ln(I_t/I_0)$, where Λ is the total mean free path for inelastic scattering, I_t and I_0 are the integral intensities of the overall spectrum and the zero-loss peak, respectively.[18] In this case, the Λ value for graphite was used. Figure 1c shows the thickness of the contamination as a function of irradiation time, indicating that the thickness of the contamination increases with the total dose given to the irradiated regions and reaches to about 600 nm with 10 min irradiation.

The sources of hydrocarbons are attributed to be vacuum pump oils, degradable or outgassing specimens, and poor vacuum practice.[19] Even under ultrahigh vacuum conditions, some of the contamination sources continue to reside inside the chamber and are not easily removable. Despite the use of oil-free pumps at all stages of the vacuum system in our microscope, the contamination sources still could not be entirely removed from the inside of the electron microscope. When electron beam is irradiated on a polymer specimen, the specimen degrades and low-molar species evaporate where some species continue to remain and end up accumulating inside the chamber as residual carbonaceous contaminations. Those accumulated contaminants again evaporated and then are re-deposited on a specimen surface where the electron beam is irradiated. The radiation-sensitive specimens contaminate the microscope, and the contaminated microscope causes the specimen contamination. This contamination vicious circle causes serious problems especially in case of soft-material imaging.

Cleaning of a Transmission Electron Microscope with Activated Oxygen Radicals. A common method for reducing the contamination rate is the use of an anticontamination device. This device cools the area around the specimen with liquid nitrogen and decreases the partial pressure of hydrocarbons. However, the contamination still cannot be sufficiently suppressed especially when small electron probes are employed for microanalysis. The use of a plasma generating system has been applied to analytical TEM and focused ion-beam (FIB) milling to minimize and, in some cases, eliminate the problems associated with various contamination sources.[20,21] In

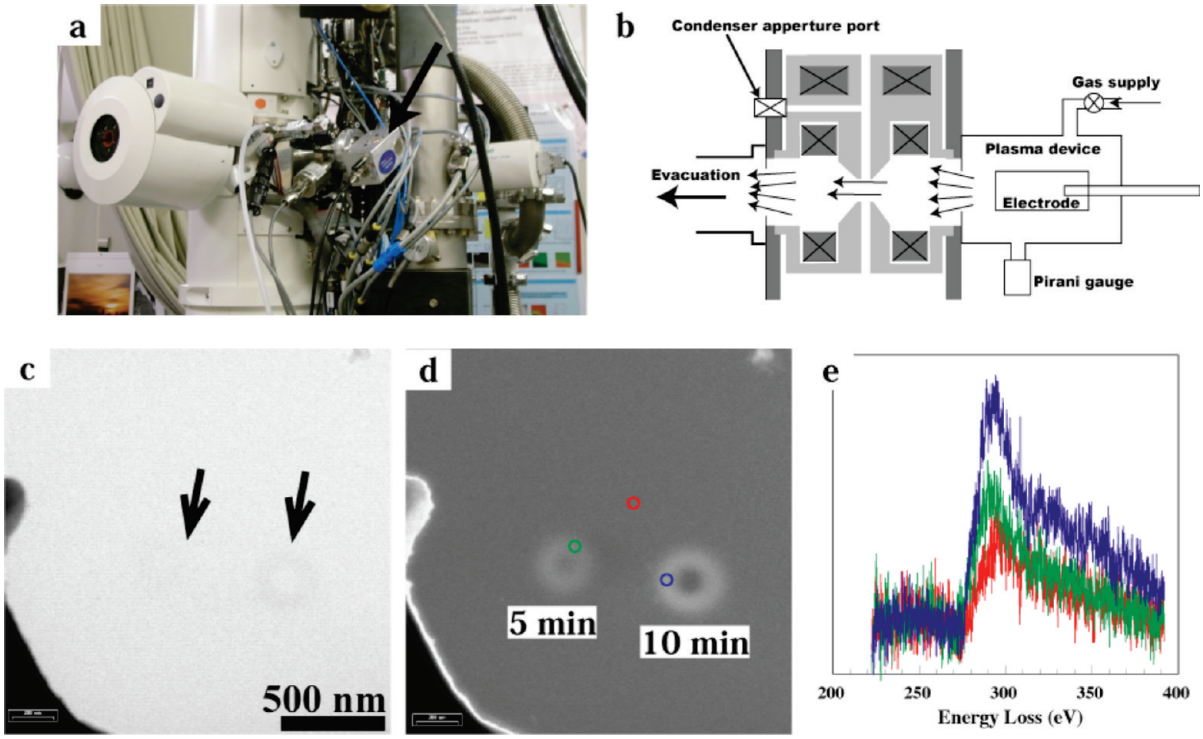

Figure 2. Cleaning of a TEM chamber using a compact plasma generator. (a) Photograph showing the plasma generator (indicated by an arrow) mounted on an accessory port close to the specimen chamber. (b) Schematic illustration showing the created flow of activated oxygen radicals in the TEM. (c) Zero-loss and (d) energy-filtered image at 50 ± 10 eV, showing the contamination marks produced on an OsO_4 thin film after the cleaning. The irradiation condition was same as employed before the cleaning. (e) Carbon K-edges acquired from the regions indicated in panel d.

such methods, the carbonaceous contamination can be effectively removed from a specimen. Electron microscopy parts and accessories, such as apertures, specimen clamping rings, and Wehnelts, can also be plasma-cleaned. However, soft materials suffer from serious structural changes by the plasma treatment, and the cleaning of the specimen holder and other parts cannot sufficiently remove the contamination sources from TEM.

We have now developed a more effective process for the cleaning of the TEM chamber by using activated oxygen radicals. Here a compact low-temperature plasma generator (Evactron 45, XEI Scientific, Inc., USA) is mounted on one of the accessory ports close to the specimen chamber as shown in Figure 2a. This device uses a low-powered RF plasma to make oxygen radicals form air that can chemically etch away the contaminations from the interior of a vacuum chamber.[22] Hydrocarbons and other organics are oxidized by the oxygen radicals to form volatile oxides that can be easily pumped out from the TEM. The plasma itself remains confined within the plasma device and prevents ion bombardment damage to the microscope. Cleaning of scanning electron microscopes (SEMs) has successfully been employed with this device where the oxygen radicals are carried out of the plasma device into the specimen chamber by convection and flux toward the roughing pump.[19,22,23] However, the beam-induced specimen contamination in the TEM cannot be reduced by the simple operation of the plasma generator as for SEMs. The reason is assumed that the specimen chamber and the vacuum path of the TEM are considerably narrow, where sufficient oxygen radicals cannot be supplied into the chamber simply by the roughing pump of the microscope. Therefore, we introduced an additional pumping system (Edwards XDi35i oil-free scroll pump) at the objective aperture port as illustrated in Figure 2b in order to create a vis-

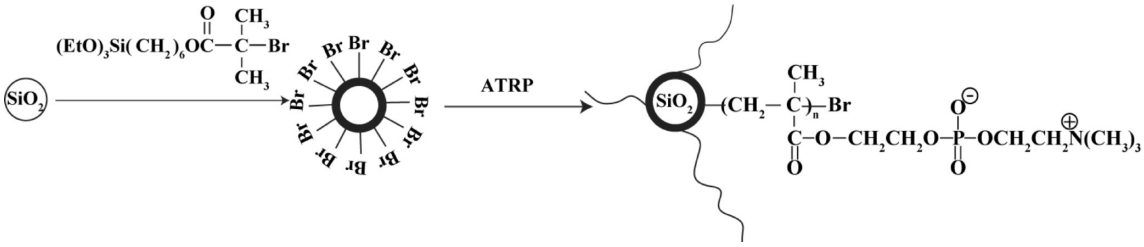

Scheme 1. Synthesis of PMPC brushes on SiNP.

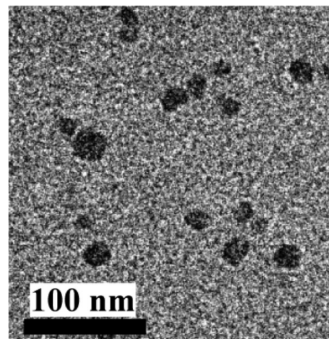

Figure 3. Global TEM image showing the distribution of PMPC-SiNPs on an OsO_4 thin film.

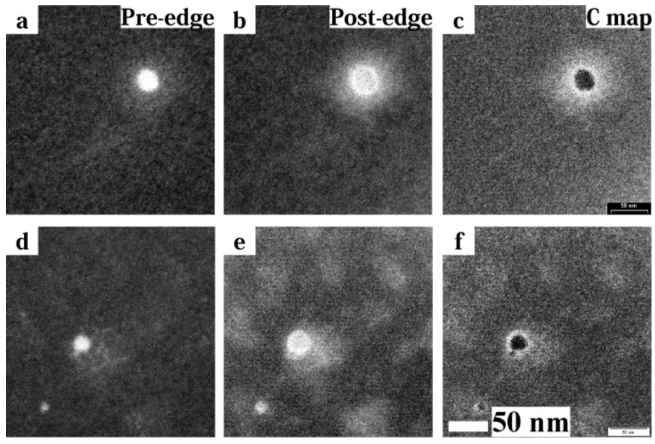

Figure 4. Carbon elemental mapping of an isolated PMPC-SiNP by EFTEM before and after the TEM cleaning. (a,d) Pre-edge images (250 ± 10 eV), (b,e) post-edge images (315 ± 10 eV), and (c,f) calculated carbon distribution images of an isolated PMPC-SiNP. Images after (a−c) and before (d−f) the cleaning.

cous flow of the oxygen radicals into the specimen chamber. In this scheme, a large amount of the oxygen radicals travels through the specimen chamber, where it can react with hydrocarbons in the chamber atmosphere and on the surfaces. The cleaning process starts with the closing of the valves to separate the column from the electron gun part and from the camera room. Also, the specimen chamber is separated from the ion-gauge pump and the turbo-molecular pump. Then, the specimen chamber was evacuated by an additional pump attached to the objective aperture port in which the pressure was kept at 0.4 Torr by a controlled leak of air into the device. After the pressure was stabilized, a high frequency power (13.56 MHz) was applied to generate the plasma under the condition of 10 W with room air as the feed gas. Gentle cleaning of the chamber was performed for 3 min, and then a nitrogen gas was purged to flush the reactant products out of the chamber at 0.9 Torr for 3 min. This cleaning/purging cycle was repeated 20 times.

After the cleaning, no contamination marks were seen even after an irradiation for 30 min of the electron beam on the carbon thin foil without the use of an anticontamination device. In a case where an osmium tetraoxide (OsO_4) plasma-polymerized thin film with the thickness of 10 nm was used as an alternative to carbon film, contamination marks created by the 5 and 10 min irradiations could be seen as extremely thin depositions and its formation could be studied by EELS, as shown in Figure 2c−e. Since the contamination consists of carbon-rich products, contrast can be enhanced when the noncarbon supporting film is used. However, the contaminations were so thin that those could hardly be seen by the zero-loss image (Figure 2c), but it could be slightly enhanced by seeing as an energy-filtered image at the 50 ± 10 eV energy losses (Figure 2d). The ring formations of the contaminations as shown in Figure 2d have been known to be caused by the surface diffusion of adsorbed hydrocarbons to the edge of the illuminated area.[3] The carbon K-edge EELS spectra shown in Figure 2e indicate that the carbon contents in the contaminations slightly increase with the irradiation period. The nonirradiated area (shown as the red mark) contains a small amount of carbon as an impurity, which might have been introduced in the film preparation process. The ratios of the integrated intensities of the carbon ionizations give the carbon atomic ratios in the measured regions.[24] The integration of the energy window of 100 eV indicates that the irradiations for 5 and 10 min increase carbon contents by 1.4 and 3 times, respectively. The carbon content in the as-prepared OsO_4 film is at trace level and is difficult to be measured. It can be mentioned that the contamination depositions were extremely thin, and the cleaning significantly could suppress the specimen contamination.

Throughout these experiments, it was revealed that the sufficient amount of the oxygen radicals should be supplied into the chamber to remove the contamination sources. High flow rate of the oxygen radicals could be achieved by appropriate operation of the plasma generator and the additional pumping system. The flow rate was 178 cm^3/min when the plasma generator and the additional pumping system were operated as illustrated in Figure 2b. On the other hand, when the plasma generator was mounted at the condenser aperture port, which is located above the specimen chamber, the flow rate was 4 cm^3/min and the specimen contamination could not be reduced.

Imaging of a Polymer Brush by Carbon Elemental Mapping. We have thus achieved the "contamination-free TEM" by gentle chemical cleaning of the specimen chamber with activated oxygen radicals without causing any damage to the microscope. To examine the advantage of the contamination-free TEM, we investigated the structure of a single polymer layer immobilized on the surface of a silica nanoparticle (SiNP) by carbon elemental mapping. The sample used in this experiment is shown in Scheme 1. The synthesis procedure of this sample has been described in detail in earlier publications: The surface initiator, (2-bromo-2-methyl)propionyloxyhexyltriethoxysilane (BHE), was immobilized

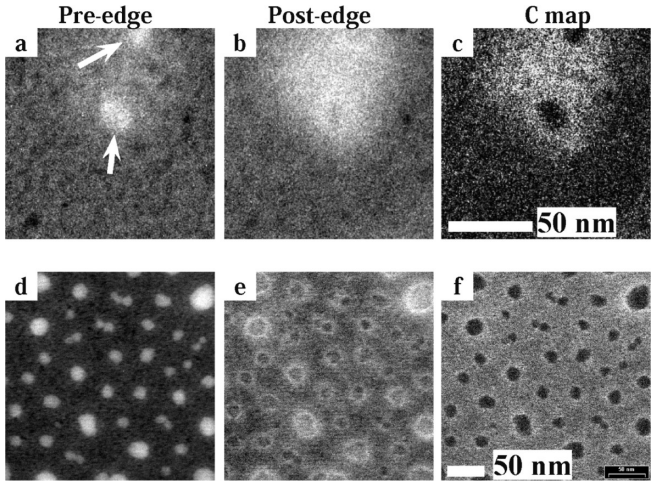

Figure 5. Carbon elemental mapping of PMPC-SiNP particles showing the interconnection of the polymer chains by two particles (a−c) and multiple particles (d−f): (a,d) pre-edge images, (b,e) post-edge image, and (c,f) carbon distribution images.

on the surface of the SiNP,[25] of which the average diameter was 12 nm (IPA-ST, Nissan Chemical Industries Ltd., Japan). Then, poly(2-methacryloyloxyethyl phosphorylcholine) (PMPC) was grafted on the BHE-immobilized SiNP by the surface-initiated atom-transfer radical polymerization.[26] The number-average molecular weight (M_n) and the graft density of the surface-grafted PMPC were determined by the thermogravimetric analysis (TGA), SEC, and NMR to be 61 000 and 0.073 chains/nm^2 (about 33 chains immobilized on 1 SiNP on average), respectively. Also, the hydrodynamic radius of PMPC-immobilized SiNP (PMPC-SiNP) in water was estimated at 48.1 nm by dynamic light scattering (DLS). The dimension of the PMPC polymer chains immobilized on SiNP is much larger than that of the corresponding free polymer, suggesting that the PMPC chains form a "polymer brush" where the radially oriented chains stretch perpendicularly against the silica surface owing to the strong intermolecular repulsive interaction of PMPC. PMPC has attracted great interests for its excellent biocompatibility,[27] and it also has superhydrophilicity, which offers excellent stability of the SiNP aqueous suspension that prevents the aggregation and precipitation.

A specimen with the PMPC-SiNP distributed on the OsO_4 thin film was obtained as shown in Figures 3, where only the SiNPs can be seen. Panels a and b of Figure 4 are energy-filtered images of an isolated particle taken at the energy losses of 270 ± 10 and 315 ± 10 eV, respectively, which correspond to the pre- and post-edge images for the carbon K-edge at 285 eV, respectively. We can see the drastic change in the contrast by an energy jump beyond the carbon K-edge, showing the presence of the PMPC brush layer outside of the SiNP. Such distinct contrast difference can be achieved only by using the noncarbon OsO_4 supporting film. Figure 4c is a carbon elemental map calculated by the three-window power law method using two pre-edge images for the background calculation at 250 ± 10 and 270 ± 10 eV energy losses. The contrast differences among the three images (Figure 4a−c) indicate that the particle shown by the pre-edge image corresponds to the silica particle only, while the post-edge image shows the entire structure of the PMPC-SiNP. All the image acquisitions were performed with the limited dose at room temperature. The preacquisition process for the adjustment of focus and camera conditions was done outside the region of interest; then the region of interest was brought under the illumination, and the three energy-filtered images were acquired with a beam intensity of 1.8 × 10^5 el/nm · s and an acquisition time of 10 s at the magnification of 80 000. The carbon distribution image clearly shows the growth of the PMPC chains from the SiNP surface that cannot be seen by conventional TEM.

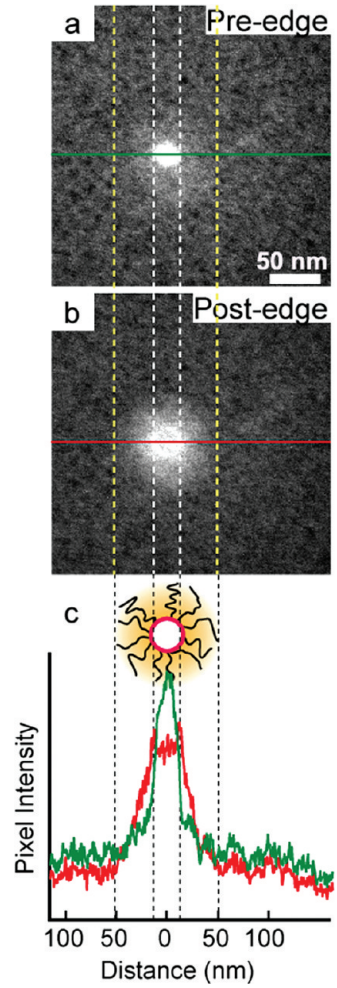

Figure 6. Pixel intensity profiles measured along the horizontal lines across the center of the PMPC-SiNP in (a) pre- and (b) post-edge images. Red and green lines in (c) correspond to the profiles obtained in (a) and (b), respectively. The illustration of the speculated structure showing the initiator and polymer brush parts is also shown in (c).

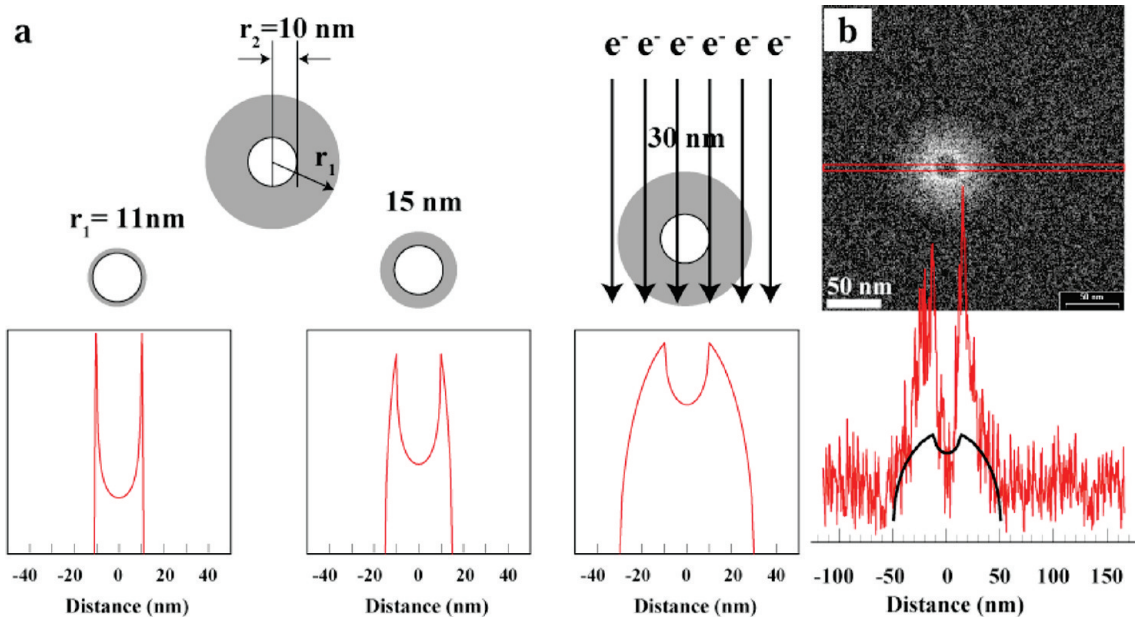

Figure 7. (a) Illustration describing the model of a core−shell particle with uniform carbon concentration in the shell and the changes in the intensity profiles with different shell thickness along the line across the particle in the projection images. (b) Carbon elemental map calculated from the pre- and post-edge images shown in Figure 6 and the measured intensity profile along the line shown in the image together with the calculated profile using the model shown in (a).

The bottom row of Figure 4 shows a series of images for the carbon elemental mapping achieved before the cleaning of the TEM. Panels d and e in Figure 4 are pre- and post-edge images for creating the carbon map, respectively, suggesting the presence of the carbon-rich layer on the SiNP surface. However, the PMPC brush layer cannot be clearly seen in the carbon distribution image (Figure 4f) due to the contamination of the irradiated region. During the irradiation of the electron beam on the specimen, thick carbon-rich deposition was formed, which obscured the PMPC brush layer. Therefore, the results strongly indicate that imaging of polymers by carbon elemental mapping is quite sensitive to the specimen contamination. The reduction of the beam-induced specimen contamination leads to significant improvement in the carbon elemental mapping. It has been generally known that the cryo-observation is effective for reducing the damage of the specimen; however, any advantage could not be found in terms of the improvement of the carbon mapping, suggesting that the cooling of the specimen may increase the contamination deposition rate.

The contamination-free TEM allows us to perform high-resolution carbon elemental mapping. We can see the formation of polymer chains extended from an silica surface, presenting the symmetrically and radially extended polymer single layer from the isolated SiNP particle. Figure 5 shows a different region of the specimen including two particles. Those two particles seem to separate from each other with the distance of about 50 nm as shown in the pre-edge image (Figure 5a), but the corresponding post-edge image (Figure 5b) and the carbon distribution image (Figure 5c) clearly indicate that the polymer brush chains are connected to each other. An about five-times concentrated aqueous solution gave a specimen with the PMPC-SiNP particles with a higher density, as shown in Figure 5d. In this case, the extended formation of the PMPC brush layers cannot be seen as was observed in the isolated particle (Figure 5e,f), suggesting that the polymer chains are entangled with each other and form a continuous film.

Dimensional Characterization of a Polymer Brush and a Surface Initiator Immobilized on a Silica Particle. The gray value intensity profiles along a horizontal line across the center of the SiNP were measured in the pre-edge and the post-edge images as shown in Figure 6a,b, respectively. The profiles measured in the two images are displayed in Figure 6c, allowing us to estimate the dimensional characteristics of the particle. The profile obtained from the pre-edge image (green line) indicates that the diameter of the SiNP is about 20 nm, while that obtained from the post-edge image (red line) estimates the PMPC brush thickness as about 40 nm. One can see the two peaks in the intensity profile of the post-edge image at the edge of the SiNP. Those sharp tiny peaks correspond to the bright ring surrounding the SiNP, as can be seen in Figure 4b, and presumably are assigned to the surface initiator (BHE) immobilized on the SiNP surface. This speculation is supported by the experimental fact that the average number of PMPC brushes grafted on a SiNP is 33 while that of the immobilized BHE is 387, which was determined by TGA.[26] This means that carbon density of the initiator is significantly higher than that of the grafted PMPC chains. Thus, the surface initiator can be differentiated from the polymer brush layer as illustrated in Figure 6c, and its thickness is estimated as about 5 nm.

Images given by TEM are two-dimensional projections of samples. In the model of core−shell particles in which the carbon concentration in the shell is uniform and the core contains no carbon, the length of the line along which the electron beam passes in the shell is proportional to the pixel intensity of the profile in the carbon map. The variation of the shell thickness with the fixed core radius at 10 nm results in the change in the profile as shown in Figure 7a, showing the tendency that the intensities under the core particle increase with increase of the shell thickness. The shape of the profile obtained from the carbon map of the PMPC-SiNP is, however, different from the calculated one, as shown in Figure 7b, suggesting that the inner side of the brush layer is more concentrated than the outer side. What we can see by the carbon elemental mapping is a dry brush adsorbed on the substrate. Therefore, the shapes and the density of the brush layer are different from those in the suspension. However, the carbon map well represents the symmetrically and radially extended brush layer with the comparable dimension as was measured by DLS.

CONCLUSIONS

We have developed a cleaning process of a TEM by gentle chemical etching of the carbonaceous contaminations accumulated inside the specimen chamber. It can effectively reduce the beam-induced specimen contamination, which dramatically improves the quality of carbon elemental maps of polymers. The polymer chains end-immobilized on the silica particles can be imaged by ESI, and its dimension can be characterized quantitatively by carbon elemental mapping. The modifications of inorganic surfaces with organic compounds have been employed for improving dispersion, wetting, and adhesion. Thus, this analytical technique could be a promising approach for various industrial materials. For the analysis of polymers by EFTEM, the detection of carbon is much simpler than those of other light elements because of its high content. Thus, an image with high signal-to-noise ratio can be obtained with lower electron doses than for other elements. Therefore, the possibility of carbon analysis by elemental mapping and EELS with high spatial resolution has the potential to lead to the advancement for soft-material nanoanalysis by EFTEM. Also, the contamination-free TEM will contribute to various analytical techniques requiring extended exposure time of electron beam, such as electron tomography, EELS, and nanobeam diffraction.

MATERIALS AND METHODS

Specimen Preparations. Electron-beam-induced specimen contamination was evaluated using carbon-coated microgrids purchased from Okenshoji Co., Ltd. (Tokyo, Japan), where 10 nm thick carbon thin foils were supported with lacey polyvinyl formal. Plasma-polymerized OsO_4 films were prepared by the DC glow charge method using a plasma coater (OP80NT, Filgen Inc., Japan). The film was deposited on a cleaved single-crystal NaCl surface for 5 s at 1.2 kV to produced 10 nm thick films. The film was lifted off the substrate by dipping into water and collected onto 2000-mesh copper grids. Five microliters of a dilute aqueous suspension of PMPC-SiNP (75 and 400 μg/mL) was dropped onto a copper grid covered with an OsO_4 film, and then it was dried *in vacuo* overnight.

EFTEM. A LEO922 energy-filtering transmission electron microscope, in which an Omega-type energy filter is integrated, was used at an accelerating voltage of 200 kV. In EFTEM, the transmitted electrons are selected not only according to their scattered angle but also according to their energy. The energy filter disperses the inelastically scattered electrons generated by electron−specimen interactions according to their energy. This enables us to perform ESI and EELS. ESI was employed for obtaining zero-loss images and carbon elemental mapping. All normal TEM images shown in this paper are zero-loss images that are formed by inserting the energy-selecting slit below the filter with the 20 eV width centered at the zero-loss peak. Carbon elemental mapping was performed in accordance with the "three-window power law" method. This method involves several steps: First, an image in the vicinity of the carbon ionization K-edge at 285 eV is acquired as an image containing element-specific information, and then two images are acquired below the absorption edge that define the background intensities. Following this, a background image below the absorption edge is computed pixel by pixel by extrapolation to the energy loss value above the absorption edge. Finally, this background image is subtracted from the element-specific image. For the creation of a background image, the background curve is modeled as the following equation:

$$I = AE^{-r} \quad (1)$$

where I is the signal intensity, E is the energy loss, and A and r are the adjustable parameters. A and r are calculated pixel by pixel from the two images below the edge. Image recording and processing was performed using a slow scan CCD camera, Proscan HSC2 (Proscan Co. Ltd.), and an image processing system, analySIS (Soft Imaging System, Co. Ltd.), on a PC connected to the microscope.

EELS spectra were acquired by "Parallel EELS" technique. In Parallel EELS, the specimen area to be analyzed was determined by inserting an aperture at the entrance of the filter. The spectrum was captured on an Imaging Plate (DITABIS, Digital Biomedical Imaging Systems AG, Germany), and the image analysis system measured the intensity and converts it into a spectrum.

Acknowledgment. Financial support was provided from the Research & Development Project for Supporting Small and Medium Enterprises by Ministry of Economy, Trade and Industry (METI), Japan. We thank K. Ishihara, University of Tokyo, for kindly supplying PMPC monomers.

REFERENCES AND NOTES

1. Kimoto, K.; Asaka, T.; Nagai, T.; Saito, M.; Matsui, Y.; Ishizuka, K. Element-Selective Imaging of Atomic Columns in a Crystal Using STEM and EELS. *Nature* **2007**, *450*, 702–704.
2. Muller, D. A.; Kourkoutis, L. F.; Murfitt, M.; Song, J. H.; Hwang, H. Y.; Silcox, J.; Dellby, N.; Krivanek, O. L. Atomic-Scale Chemical Imaging of Composition and Bonding by Aberration-Corrected Microscopy. *Science* **2008**, *319*, 1073–1076.
3. Reimer, L. *Transmission Electron Microscopy*; Springer: Heidelberg, Berlin, Germany, 1997; pp 488−494.
4. Malac, M.; Beleggia, M.; Taniguchi, Y.; Egerton, R. F.; Zhu, Y. Low-Dose Performance of Parallel-Beam Nanodiffraction. *Ultramicroscopy* **2008**, *109*, 14–21.
5. Kim, G.; Sousa, A.; Meyers, D.; Shope, M.; Libera, M.

Diffuse Polymer Interfaces in Lobed Nanoemulsions Preserved in Aqueous Media. *J. Am. Chem. Soc.* **2006**, *128*, 6570–6571.
6. Yakovlev, S.; Libera, M. Dose-Limited Spectroscopic Imaging of Soft Materials by Low-Loss EELS in the Scanning Transmission Electron Microscope. *Micron* **2008**, *39*, 734–740.
7. Linares, E. M.; Leite, C. A. P.; Valadares, L. F.; Silva, C. A.; Rezende, C. A.; Galembeck, F. Molecular Mapping by Low-Energy-Loss Energy-Filtered Transmission Electron Microscopy Imaging. *Anal. Chem.* **2009**, *81*, 2317–2324.
8. Liao, Y.; Nakagawa, A.; Horiuchi, S.; Ougizawa, T. Interdiffusion at Homopolymer/Random Copolymer Interfaces Investigated by Energy-Filtering Transmission Electron Microscopy. *Macromolecules* **2007**, *40*, 7966–7972.
9. Horiuchi, S.; Dohi, H. Nanoimaging and Spectroscopic Analysis of Rubber/ZnO Interfaces by Energy-Filtering Transmission Electron Microscopy. *Langmuir* **2006**, *22*, 4607–4613.
10. Liao, Y.; Horiuchi, S.; Nunoshige, J.; Akahoshi, H.; Ueda, M. Reaction-Induced Phase Decomposition of Thermoset/Thermoplastic Blends Investigated by Energy Filtering Transmission Electron Microscopy. *Polymer* **2007**, *48*, 3749–3758.
11. Horiuchi, S.; Yin, D.; Liao, Y.; Ougizawa, T. Study of Adhesion and Fracture of Polymer Laminates by Imaging of Interfaces. *Macromol. Rapid Commun.* **2007**, *28*, 915–921.
12. Kumao, A.; Hashimoto, H.; Shiraishi, K. Studies on Specimen Contamination by Transmission Electron Microscopy. *J. Electron Microsc.* **1981**, *30*, 161–170.
13. Fan, X.; Lin, L.; Messersmith, P. B. Cell Fouling Resistance of Polymer Brushes Grafted from Ti Substrates by Surface-Initiated Polymerization: Effect of Ethylene Glycol Side Chain Length. *Biomacromolecules* **2006**, *7*, 2443–2448.
14. Kobayashi, M.; Terayama, Y.; Hosaka, N.; Kaido, M.; Suzuki, A.; Yamada, N.; Torikai, N.; Ishihara, K.; Takahara, A. Friction Behavior of High-Density Poly(2-methacryloyloxyethyl phosphorylcholine) Brush in Aqueous Media. *Soft Matter* **2007**, *3*, 740–746.
15. Ohno, K.; Morinaga, T.; Takeno, S.; Tsujii, Y.; Fukuda, T. Suspensions of Silica Particles Grafted with Concentrated Polymer Brush: A New Family of Colloidal Crystals. *Macromolecules* **2006**, *39*, 1245–1249.
16. Ohno, K.; Morinaga, T.; Takeno, S.; Tsujii, Y.; Fukuda, T. Suspensions of Silica Particles Grafted with Concentrated Polymer Brush: Effects of Graft Chain Length on Brush Layer Thickness and Colloidal Crystallization. *Macromolecules* **2007**, *40*, 9143–9150.
17. Mizutani, A.; Kikuchi, A.; Yamato, M.; Kanazawa, H.; Okano, T. Preparation of Thermoresponsive Polymer Brush Surfaces and Their Interaction with Cells. *Biomaterials* **2008**, *29*, 2073–2081.
18. Egerton, R. F. *Electron Energy-Loss Spectroscopy in the Electron Microscope*; Plenum Press: New York, 1996, pp 301−312.
19. Vladár, A. E.; Postek, M. T.; Vane, R. Active Monitoring and Control Electron Beam Induced Contamination. *Proc. SPIE* **2001**, *4344*, 835–843.
20. Sullivan, N.; Mai, T.; Bowdoin, S.; Vane, R. A. Study of the Effectiveness of the Removal of Hydrocarbon Contamination by Oxidative Cleaning inside the SEM. *Microsc. Microanal.* **2002**, *8*, 720–721.
21. Isabell, T. C.; Fischione, P. E.; O'Keefe, C.; Guruz, M. U.; Dravid, V. P. Plasma Cleaning and Its Applications for Electron Microscopy. *Microsc. Microanal.* **1999**, *5*, 126–135.
22. Hata, S.; Sosiati, H.; Kuwano, N.; Itakura, M.; Nakano, T.; Umakoshi, Y. J. Removing Focused Ion-Beam Damages on Transmission Electron Microscopy Specimens by Using a Plasma Cleaner. *J. Electron Microsc.* **2006**, *55*, 23–26.
23. Vane, R.; Carlino, V. Environmental Contamination Sources and Control in High Resolution Scanning Electron Microscopy. *Microsc. Microanal.* **2005**, 900–901.
24. Leapman, R. In *Transmssion Electron Energy Loss Spectrometry in Materials Science and the EELS ATLAS*; Ahn, C., Ed.; Wiley-VCH: Weinheim, Germany, 2004; p 4996.
25. Ohno, K.; Morinaga, T.; Tsujii, Y.; Fukuda, T. Synthesis of Monodisperse Silica Particles Coated with Well-Defined, High-Density Polymer Brushes by Surface-Initiated Atom Transfer Radical Polymerization. *Macromolecules* **2005**, *38*, 2137–2142.
26. Matsuda, Y.; Kobayashi, M.; Annaka, M.; Ishihara, K.; Takahara, A. Dimensions of a Free Linear Polymer and Polymer Immobilized on Silica Nanoparticles of a Zwitterionic Polymer in Aqueous Solutions with Various Ionic Strengths. *Langmuir* **2008**, *24*, 8772–8778.
27. Ishihara, K.; Ueda, T.; Nakabayashi, N. Preparation of Phospholipid Polymers and Their Properties as Polymer Hydrogel Membranes. *Polym. J.* **1990**, *22*, 355–360.